



**Structural Transformation of Metal Oxo Species within UiO-66 Type Metal–Organic Frameworks**

Journal:	<i>CrystEngComm</i>
Manuscript ID	CE-ART-05-2022-000650.R1
Article Type:	Paper
Date Submitted by the Author:	21-Jun-2022
Complete List of Authors:	Wasson, Megan; Northwestern University, Xie, Haomiao; Northwestern University Wang, Xingjie; Northwestern University, Chemistry Duncan, Joshua; Northwestern University Farha, Omar; Northwestern University, Chemistry

# Structural Transformation of Metal Oxo Species within UiO-66 Type Metal–Organic Frameworks

Megan C. Wasson, Haomiao Xie, Xingjie Wang, Joshua S. Duncan, and Omar K. Farha\*

Affiliation: International Institute for Nanotechnology and Department of Chemistry, Northwestern University, 2145 Sheridan Road, Evanston, Illinois 60208, United States

**Abstract:** Studying the coordination of actinide-based metal oxo clusters can provide valuable insights for nuclear energy technologies and radioactive waste containment. Metal–organic frameworks serve as a platform to directly interrogate the structure and properties of understudied actinide elements, including thorium. Examples of structural evolutions within Th oxo species within MOFs are rare yet relevant for nuclear waste speciation in solution. Herein, we report the serendipitous discovery of the structural evolution of Th-UiO-66 containing a hexanuclear Th node to a mononuclear  $\text{Th}(\text{bdc})_2(\text{dmf})_2$  upon the evaporation of solvent from the reaction. We observe a partial reversal of  $\text{Th}(\text{bdc})_2(\text{dmf})_2$  back to Th-UiO-66 upon hydrothermal treatment, indicating the complex dynamics of Th oxo species in solution. We report that isolated Ce-UiO-66 similarly transforms to a newly isolated 1D  $\text{Ce}^{\text{III}}$  carboxylate chain MOF named NU-351 in the same conditions as Th-UiO-66, while Zr-UiO-66 and Hf-UiO-66 retain their structures.

## Introduction

Metal–organic frameworks (MOFs) are an emerging class of highly porous, well-defined crystalline materials that have attracted considerable interest for catalysis, gas storage/separation, toxic chemical sequestration, and chemical sensing, among other applications.<sup>1–5</sup> Inorganic nodes, comprised of either metal ions or metal clusters, form coordination bonds to multitopic organic linkers to produce a targeted MOF. Researchers can leverage this tunability to impart and study

targeted chemical reactivity within the different building units. Moreover, the controlled self-assembly of the MOF building blocks can spatially isolate components to better study or harness their chemical properties.

Beyond the well-studied transition metal elements ubiquitous within MOF literature, recent reports of actinide-containing MOF nodes have accelerated the understanding of the elements' unique coordination chemistry which is pertinent for the nuclear waste storage and nuclear energy applications.<sup>6–15</sup> In particular, limited knowledge exists about that solid-state structural chemistry of thorium due to the uncontrolled growth of polynuclear Th species in solution.<sup>16,17</sup> Recent interest has surfaced to better understanding the structural behavior of thorium given surging interest in developing a more sustainable nuclear fuel process based on the  $^{233}\text{U}$ – $^{232}\text{Th}$  fuel cycle as opposed to the  $\text{U}^{235}$  fuel cycle.<sup>18,19</sup> Furthermore,  $\text{Th}^{\text{IV}}$  is largely considered a surrogate to study the coordination and behavior of more highly regulated  $\text{Pu}^{\text{IV}}$ .<sup>20</sup>

Approximately 60 thorium oxide-based coordination compounds have been reported in the Cambridge Structural Database, which appears miniscule as compared to the vast number of total coordination compounds deposited.<sup>21</sup> Therefore, a major impetus is directed at expanding the library of thorium-oxo based clusters and frameworks through systematically tuning solvent compositions and reagent ratios.<sup>22,23</sup> For example, modifying the concentration of selenic acid and water in the presence of thorium hydrates yielded 5 discrete Th clusters; lowered reaction temperature and acidity yielded higher nuclearity Th clusters.<sup>21</sup> Seminal work by Volkringer, Loiseau, and co-workers further accessed Th oxo clusters installed within Th-based MOFs, including a Th analogue of the well-known Zr-MOF UiO-66,<sup>24</sup> through the modulation of temperature, Th: linker ratio, and water concentration.<sup>25</sup> Th-UiO-66 features a  $\text{Th}_6\text{O}_8$  building block previously isolated as a discrete Th oxo cluster.<sup>26–28</sup> Alternatively, Th-based MOFs can

stabilize unique cluster coordination elusive within discrete thorium clusters. For example, our group reported a hexanuclear secondary building unit comprised of  $[\text{Th}_6(\mu_3\text{-O})_2(\text{HCOO})_4(\text{H}_2\text{O})_6]$  self-assembled with tetrakis(4-carboxyphenyl)porphyrin linkers.<sup>29</sup> However, once Th-based frameworks are assembled, examples of structural evolution within Th-based MOFs are rare. In one recent study, a non-interpenetrated MOF dissolved and recrystallized into a 2-fold interpenetrated MOF, but the Th nuclearity of the node remained the same.<sup>30</sup> Therefore, it is imperative to study examples of Th-MOF based phase transformation with the evolution of the Th oxo species better understand the coordination chemistry of Th.

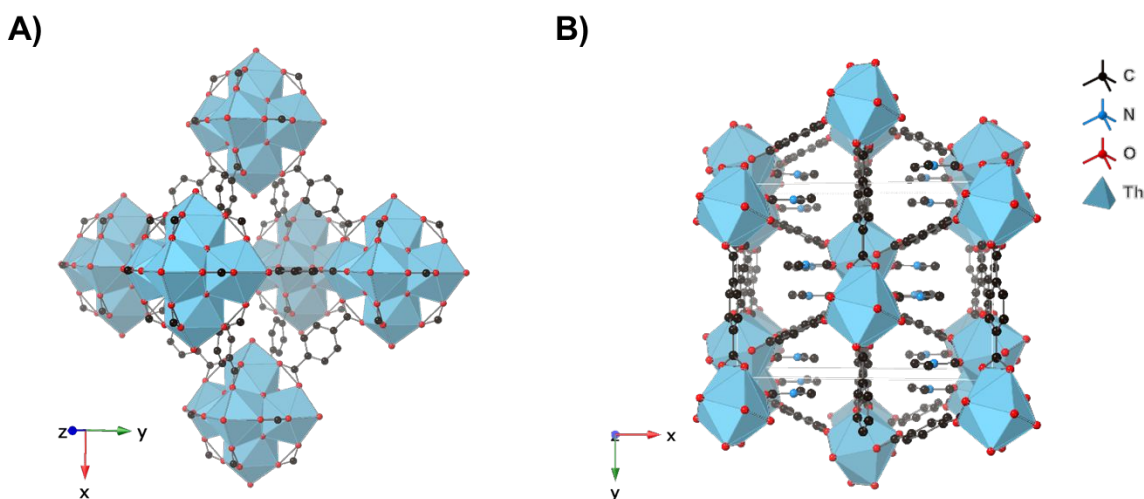


**Figure 6.1** Structures of (A) Th-UiO-66 and (B) Th(bdc)<sub>2</sub>(dmf)<sub>2</sub>.

Herein, we report the discovery of a phase transition between Th-UiO-66 and Th(bdc)<sub>2</sub>(dmf)<sub>2</sub> over time. This transition is accompanied by the hydrolysis of the Th<sub>6</sub>O<sub>8</sub> node of Th-UiO-66 to a 10-coordinate ThO<sub>8</sub>(dmf)<sub>2</sub> node. We monitored the process over 72 hr with powder X-ray diffraction (PXRD) and scanning electron microscopy (SEM) techniques. We postulate that that solvent evaporation and subsequent increased concentration of reagents in solution result in the phase transition. Moreover, the transition is suggested to be partially reversible upon the

addition of heat and water to  $\text{Th}(\text{bdc})_2(\text{dmf})_2$  to partially reform Th-UiO-66. Under the same conditions that Th-UiO-66 transitions, its isostructural Ce-UiO-66 analogue also transforms into a newly reported 1D  $\text{Ce}^{\text{III}}$  carboxylate MOF, NU-351, while Zr-UiO-66 and Hf-UiO-66 retain their structures.

## Results and Discussion

We serendipitously observed a phase transition of Th-UiO-66 to the reported  $\text{Th}(\text{bdc})_2(\text{dmf})_2$  polymorph when the reaction time was increased from 24 hr to 72 hr (**Figure 1**). In 2 separate trials, identical solutions of 0.9 mmol 1,4 benzene dicarboxylic acid and 0.35 mmol  $\text{Th}(\text{NO}_3)_4 \cdot 5\text{H}_2\text{O}$  were reacted for 24 hr and 72 hr in a 4:1 solution of DMF: water. The resulting PXRD patterns demonstrated good agreement of the 24 hr synthesis with the simulated Th-UiO-66 pattern while the 72 hr synthesis matched the simulated pattern of  $\text{Th}(\text{bdc})_2(\text{dmf})_2$  (**Figure S1**). While the initial report of Th-UiO-66 included thorough synthetic screenings to yield the MOFs in pure-phase, a transition from one phase to another over time was not explored.<sup>25</sup> We were intrigued by the hydrolysis of the  $\text{Th}_6\text{O}_8$  node of Th-UiO-66 to a 10-coordinate  $\text{ThO}_8(\text{dmf})_2$  node and further investigated the kinetic timescale of this transition.

PXRD patterns were collected of identical solutions and each vial was removed after 12 hours to monitor the crystalline phase formed. As shown in **Figure 6.2**, we observed PXRD patterns from 12-48 hr that are consistent with Th-UiO-66. After 60 hours, the growth of Th(bdc)<sub>2</sub>(dmf)<sub>2</sub> peaks was indicated through the appearance of five new peaks at between 10-13 degrees 2θ, while the primary Th-UiO-66 peaks at 6.9 and 7.9 degrees 2θ are still visible. The PXRD pattern collected at 72 hours demonstrated a nearly complete conversion of Th-UiO-66 to the Th(bdc)<sub>2</sub>(dmf)<sub>2</sub> framework. SEM images complemented the growth of Th(bdc)<sub>2</sub>(dmf)<sub>2</sub> after 60 hours with the presence of large 100 μm size trapezoidal crystals appearing along size of smaller 1 μm sized Th-UiO-66 particles. The larger 100 μm trapezoidal crystals of Th(bdc)<sub>2</sub>(dmf)<sub>2</sub> were only observed at 72 hr. After 72 hr, the reaction vials contained ~ 50% of the starting solvent amount (approximately 2.5 mL), indicating solvent evaporation must have occurred during the solvothermal synthesis.

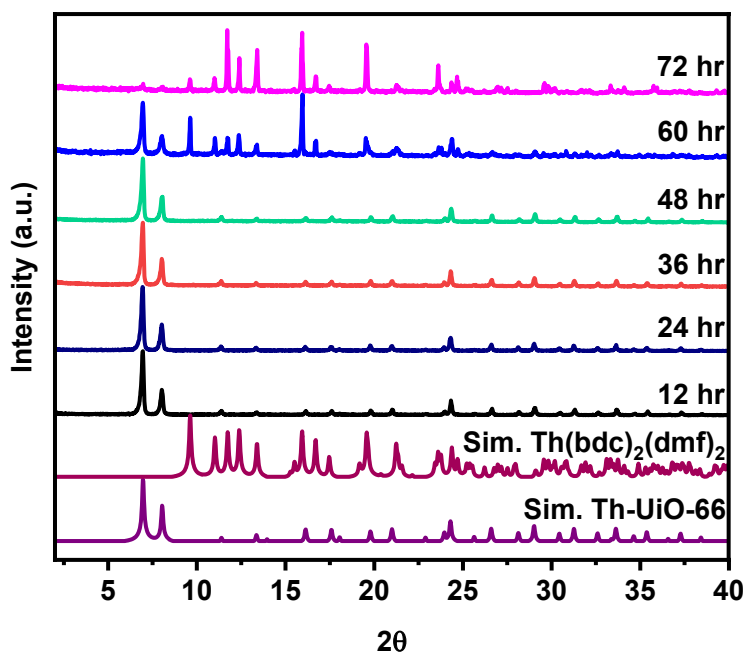


**Figure 2:** PXRD patterns of phase transition monitored of Th-UiO-66 to Th(bdc)<sub>2</sub>(dmf)<sub>2</sub> at a designated time point of the reaction between 1,4 benzene dicarboxylic acid and Th(NO<sub>3</sub>)<sub>4</sub>·5H<sub>2</sub>O.

Beyond the different node environments, the two MOFs have vastly different physical

properties as evidenced through surface areas of 620 m<sup>2</sup>/g for Th-UiO-66 compared to < 5 m<sup>2</sup>/g

for  $\text{Th}(\text{bdc})_2(\text{dmf})_2$  (**Figures S8-S9**). Thus, it is imperative to better understand the complexity of

the phase transformation. We then sought to complete *in situ* investigations to monitor the phase

transitions. Before observing the 72-hour process *in situ*, we first took an aliquot of the reaction mixture (see supporting information) and placed it in a borosilicate capillary that was flame sealed. We compared the PXRDs of the capillary heated in the oven concurrently with the mother reaction mixture in a vial reacting at the same time. After 72 hours, PXRDs demonstrated that the flame sealed system formed Th-UiO-66 while the mother solution in the vial formed  $\text{Th}(\text{bdc})_2(\text{dmf})_2$  (**Figure S2**). Thus, we reasoned that the flame seal capillary must provide a better seal for our reactants than the polyvinyl capped vials our bulk syntheses were conducted in, which resulted in the aforementioned solvent evaporation over the reaction time. We conjectured that a higher concentration of reactants results in the formation of  $\text{Th}(\text{bdc})_2(\text{dmf})_2$ .

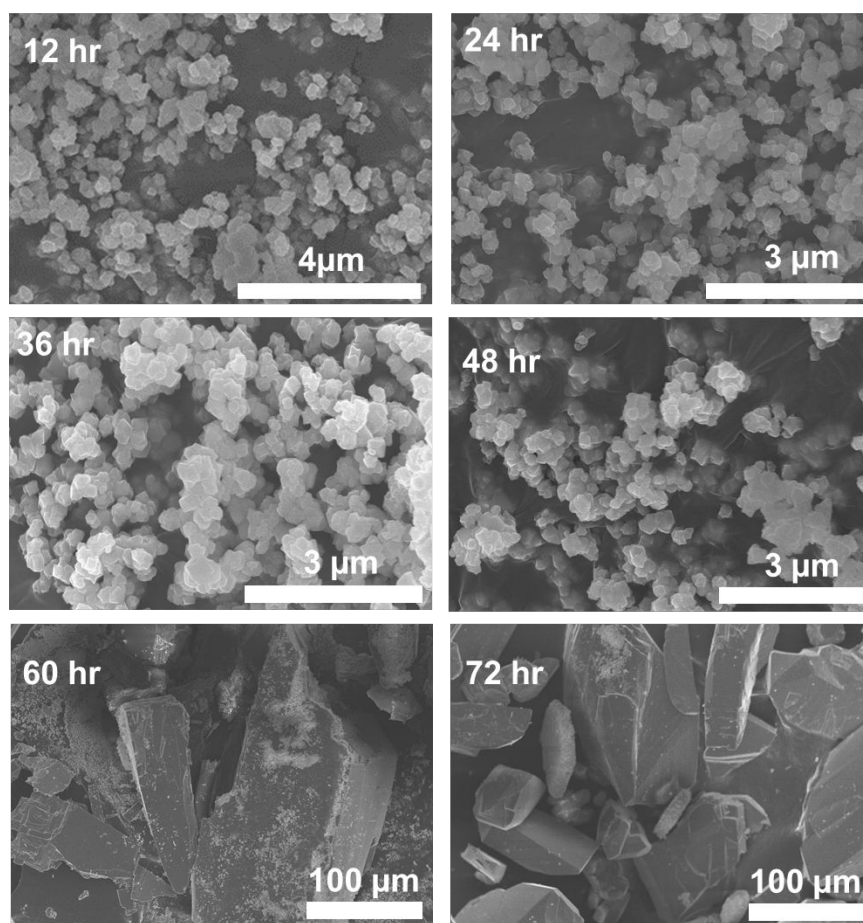


**Figure 3:** SEM images of resulting particles from the reaction between 1,4 benzene dicarboxylic acid and  $\text{Th}(\text{NO}_3)_4 \cdot 5\text{H}_2\text{O}$  at designated time points.

In our next set of experiments, we used vials with caps lined with polytetrafluoroethylene (PTFE) which features a higher melting point than polyvinyl, providing a more closed system and limiting solvent evaporation. We utilized the same amount of reagents and ratio of DMF: water in the solution as our prior experiments, but systematically decreased the total solvent amount to increase the overall concentration of both reactants in solution. The syntheses reacted again for 72 hr, and we utilized PXRD to investigate the resulting phases. We observed the most visible formation of  $\text{Th}(\text{bdc})_2(\text{dmf})_2$  with the highest concentration (3x) of the reactants (pattern C in **Figure S3**) while we observe a slight formation of  $\text{Th}(\text{bdc})_2(\text{dmf})_2$  in the 2x and regular concentrations in patterns B and A respectively. We determined that concentration is a critical factor in this phase transformation, but we did not observe the full conversion even in the 3x concentration vial to  $\text{Th}(\text{bdc})_2(\text{dmf})_2$ .

Given prior reports of the role of formate concentration on Th oxo cluster size, we next explored the role of the decomposition products, formic acid and dimethylamine, on the phase transition.<sup>22</sup> We added equivalents of lithium formate or a diethylamine (DEA) to isolated Th-UiO-66 added into the DMF/water solution which soaked for 48 hours at 130 °C. Through PXRDs of the resulting products, we observed only a slight formation of  $\text{Th}(\text{bdc})_2(\text{dmf})_2$  upon the addition of DEA, even with as high of a ratio of 1:1 DMF: DEA (pattern H **Figure S5**). Furthermore, solutions containing Th-UiO-66 with added lithium formate did not exhibit a phase change. We thus determined that the concentration of the reactants greatly promotes the conversion of Th-UiO-66 to  $\text{Th}(\text{bdc})_2(\text{dmf})_2$  as opposed to the decomposition products of DMF.

Previously, it was reported that water can stabilize the hexanuclear cluster of Th-UiO-66 by favoring olation and oxolation condensation processes.<sup>25</sup> Thus, we probed whether adding water to an isolated sample of  $\text{Th}(\text{bdc})_2(\text{dmf})_2$  would prompt a phase transition back to Th-UiO-66. After heating at 80 °C for 24 hr, we observed the growth of peaks at 6.9 and 7.9 degrees  $2\theta$ , consistent with the Th-UiO-66 phase as well as sharp peaks still present at 9.5 degrees  $2\theta$  and absence of higher angle peaks, indicating the retention of a  $\text{Th}(\text{bdc})_2$  framework without DMF also previously reported by Volkringer, Loiseau, and co-workers (**Figure 4**).<sup>25</sup> We attempted longer reaction times of  $\text{Th}(\text{bdc})_2(\text{dmf})_2$  in water in an attempt to fully convert the mononuclear MOF back to Th-UiO-66, but we were unable to achieve full conversion. Nonetheless, we learned that

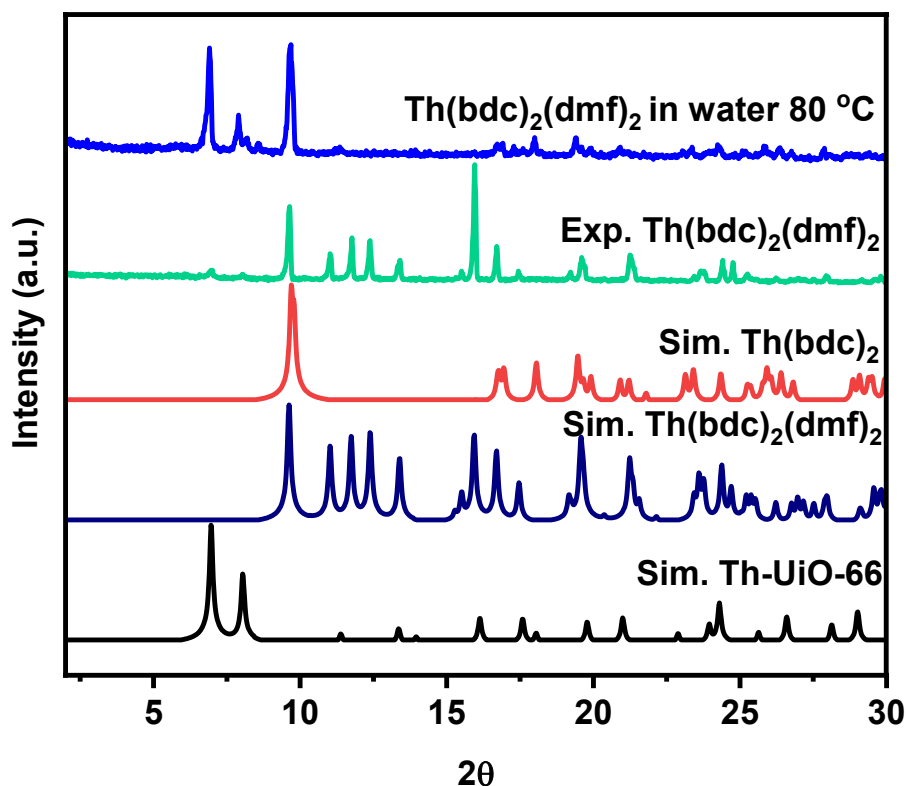


**Figure 4:** Overlaid PXRDs of  $\text{Th}(\text{bdc})_2(\text{dmf})_2$  as synthesized and after exposure to water at 80 °C for 24 hr.

the phase change is partially reversible, highlighting the complexity of Th oxo species.

Inspired by the transition between MOFs containing Th and the BDC linker, we explored whether phase transformations in other M-UiO-66 type MOFs could occur under the same conditions that facilitated the phase transition of Th-UiO-66. For example, the 1D Zr carboxylate chain MOF (MIL-140A) can also be formed from  $ZrCl_4$  and BDC linkers react as opposed to the much more well-known Zr-UiO-66 phase.<sup>31</sup> To compare the stabilities of the isostructural  $M_6O_8$  clusters, we synthesized pure-phase Zr-UiO-66, Hf-UiO-66, and Ce-UiO-66. Each MOF was heated at 130 °C in a solution of 4:1 DMF/ H<sub>2</sub>O for 48 hr to replicate the Th-UiO-66 to Th(bdc)<sub>2</sub>(dmf)<sub>2</sub> phase transition conditions. After this treatment, the PXRD patterns of Zr-UiO-66 and Hf-UiO-66 were unchanged (**Figures S6-S7**) indicating neither  $M_6O_8$  node was hydrolyzed. However, after the treatment of Ce-UiO-66, the resulting PXRD indicated the formation of a new,

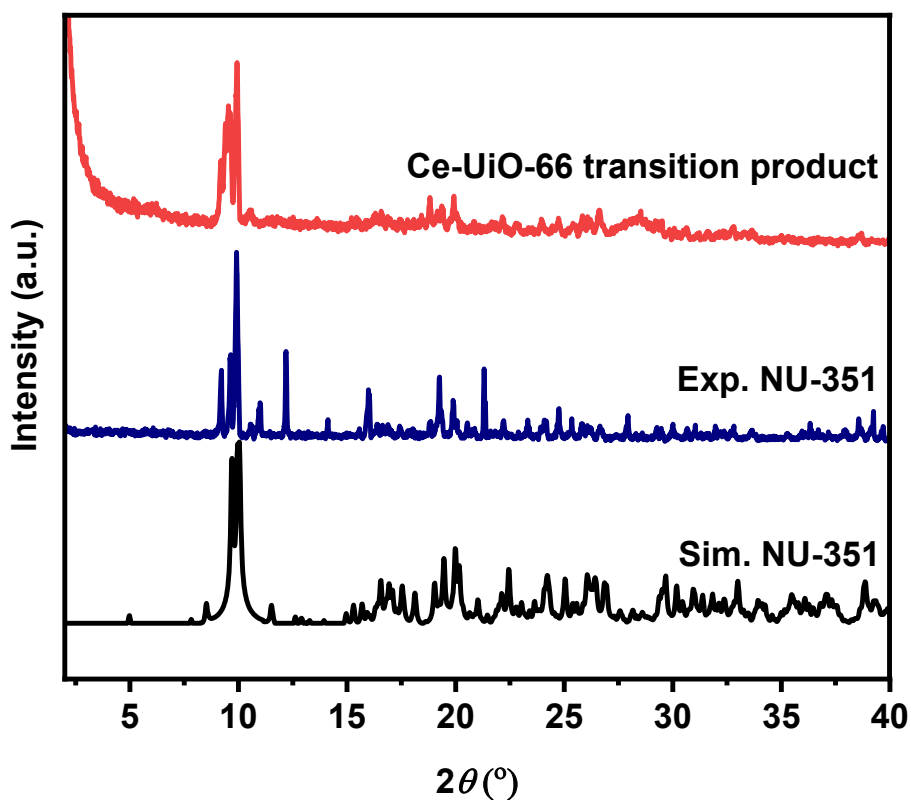


**Figure 5:** Overlaid PXRD patterns of the simulated and experimental NU-351 in agreements with the resulting phase transition of Ce-UiO-66 in 4:1 DMF/ water at 130 °C for 48 hr.

crystalline phase (**Figure 5**). Through synthetic screenings of a Ce<sup>IV</sup> source and the BDC linker, we generated single crystals of a new material called NU-351 (see synthesis in supplemental information). The experimental PXRD of NU-351 aligns with the product of the Ce-UiO-66 phase transition (**Figure 5**), and we determined the structure of NU-351 through single-crystal X-ray diffraction. As shown in **Figure 6**, NU-351 is a mononuclear Ce(III)-based MOF with the formula of (Ce<sup>III</sup>)<sub>5</sub>(BDC)<sub>7.5</sub>(DMF)<sub>5</sub> comprised of 5 crystallographically unique Ce atoms. The Ce<sup>III</sup> oxidation state was confirmed through X-ray photoelectron spectroscopy (**Figure S10**). Of note, NU-351 is structurally similar to NU-350, a mononuclear Ce<sup>III</sup>-MOF we previously reported that is favored over Ce-UiO-NDC (NDC = 2,6-naphthalenedicarboxylic acid) in the presence of low amounts of carboxylate modulator.<sup>32</sup> Thermogravimetric analyses of the two pairs of polymorphs (Th-UiO-66 / Th(bdc)<sub>2</sub>(dmf)<sub>2</sub> and Ce-UiO-66 / NU-351) were conducted to compare the thermal stabilities. Th-UiO-66 and Th(bdc)<sub>2</sub>(dmf)<sub>2</sub> exhibited similar decomposition temperatures around 500 C, which could help explain the phase reversibility of the two frameworks (**Figure S11**). However, Ce-UiO-66 decomposed beginning around 300 °C as opposed to NU-351 which remained stable until ~400 °C (**Figure S12**), which could help to rationalize the transformation of Ce-UiO-66 into the Ce polymorph of NU-351 in our studied conditions.

We postulate that the mononuclear MOFs formed from the transition of both Ce and Th-UiO-66 as opposed to Zr and Hf-UiO-66 result from several factors. Previous work from our group investigated the O-H stretching frequencies within M-UiO-66 (M= Zr, Hf, Ce, and Th) and determined that Ce and Th are less electronegative than Zr and Hf within the isostructural MOF family.<sup>33</sup> Thus, the Ce-O and Th-O bonds within the M<sub>6</sub>O<sub>8</sub> clusters are weaker than Zr-O and Hf-O, rationalizing the susceptibility of the Ce and Th nodes to undergo hydrolysis and a subsequent phase transition. Additionally, Ce and Th have larger ionic radii and increased abilities to

accommodate higher coordination numbers, likely facilitating the transition to the mononuclear MOFs with high Ce and Th coordination spheres. Lastly,  $\text{Ce}^{\text{IV}}$  has a high redox potential and can readily be reduced to  $\text{Ce}^{\text{III}}$  in DMF without sufficient modulator present, while TGA data indicated NU-351 is a more thermally stable framework than Ce-UiO-66.

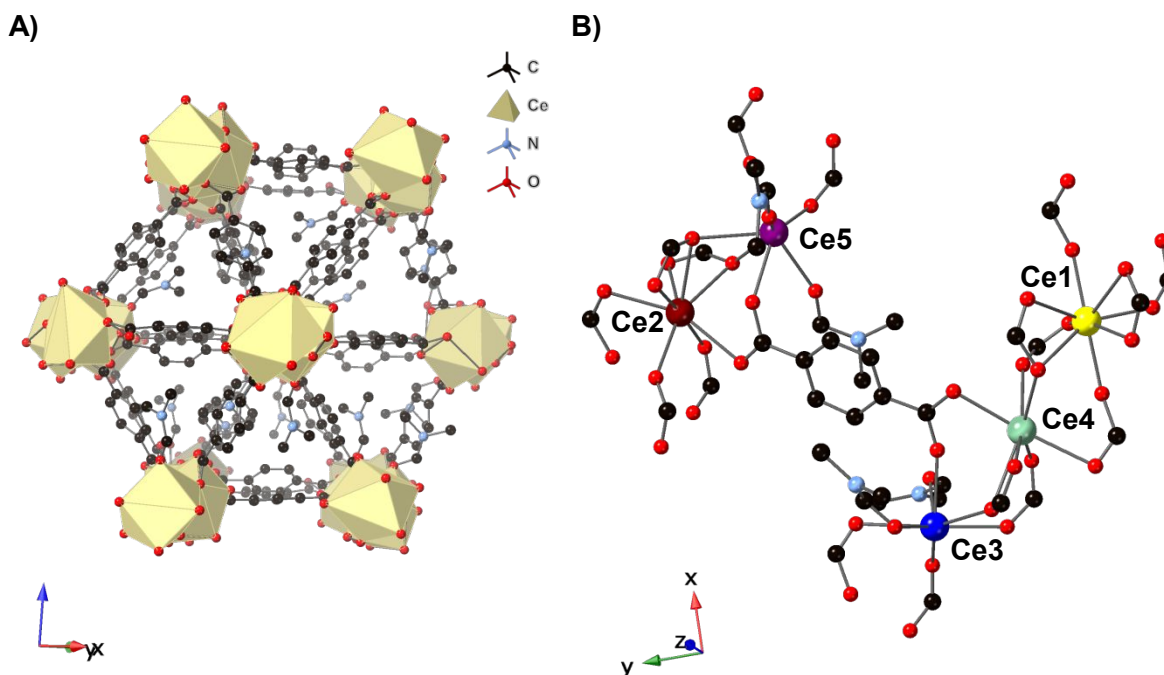


**Figure 6:** A) NU-351 structure with H atoms omitted for clarity and B) coordination environment of the 5 crystallographically distinct Ce atoms present. BDC linkers reduced to  $\text{COO}^-$  groups on node for visual clarity. Colors indicated in legend except Ce1 denoted as yellow, Ce2 denoted as dark red, Ce3 denoted as royal blue, Ce4 denoted as light green, Ce5 denoted as purple.

## Conclusions

We reported and monitored a serendipitous observation of a phase transition of Th-UiO-66 to  $\text{Th}(\text{bdc})_2(\text{dmf})_2$  through PXRD and SEM imaging, attributed to a fluctuation in concentration dependent on the reaction vial used. Furthermore, we demonstrated that the partial reversibility of

Th(bdc)<sub>2</sub>(dmf)<sub>2</sub> converting back to Th-UiO-66. Under these conditions that facilitate the phase transformation of Th-UiO-66, we determined that Ce-UiO-66 also undergoes a phase transition to NU-351 while both Zr and Hf-UiO-66 retain their structures. This work demonstrates the importance of studying the evolution of isolated metal oxo species within MOFs for both applied and fundamental perspectives; changes in Th speciation in solutions are relevant for long-term nuclear waste storage while analyzing transitions in isostructural MOFs can provide insights into overall metal oxo cluster strength and stability.

**Funding:** The authors gratefully acknowledge the Northwestern University Institute for Catalysis in Energy Processes (ICEP), funded by the DOE, Office of Basic Energy Sciences (award number DE-FG02-03ER15457). O.K.F. acknowledges support from the U.S. Department of Energy, National Nuclear Security Administration, under Award DE-NA0003763. M.C.W. is supported by the NSF Graduate Research Fellowship under grant DGE-1842165. This work made use of the IMSERC X-ray facility at Northwestern University, which has received support from the Soft and Hybrid Nanotechnology Experimental (SHyNE) Resource (NSF ECCS-1542205), the State of Illinois, and the International Institute for Nanotechnology (IIN). Also, this work made use of the Keck-II facility of Northwestern University's NUANCE Center, which has received support from the Soft and Hybrid Nanotechnology Experimental (SHyNE) Resource (NSF ECCS-1542205); the MRSEC program (NSF DMR-1720139) at the Materials Research Center; the International Institute for Nanotechnology (IIN); the Keck Foundation; and the State of Illinois, through the IIN.

**Conflicts of interest:** Omar K. Farha has a financial interest in NuMat Technologies, a company that seeks to commercialize MOFs.

## References

- 1 J. Lee, O. K. Farha, J. Roberts, K. A. Scheidt, S. T. Nguyen and J. T. Hupp, *Chem. Soc. Rev.*, 2009, **38**, 1450–1459.
- 2 H.-C. Zhou, J. R. Long and O. M. Yaghi, *Chem. Rev.*, 2012, **112**, 673–674.
- 3 R.-B. Lin, L. Li, H.-L. Zhou, H. Wu, C. He, S. Li, R. Krishna, J. Li, W. Zhou and B. Chen, *Nat. Mater.*, 2018, **17**, 1128–1133.
- 4 X. Cui, K. Chen, H. Xing, Q. Yang, R. Krishna, Z. Bao, H. Wu, W. Zhou, X. Dong, Y. Han, B. Li, Q. Ren, M. J. Zaworotko and B. Chen, *Science (80-. )*, 2016, **353**, 141 LP – 144.
- 5 J. A. Mason, J. Oktawiec, M. K. Taylor, M. R. Hudson, J. Rodriguez, J. E. Bachman, M. I. Gonzalez, A. Cervellino, A. Guagliardi, C. M. Brown, P. L. Llewellyn, N. Masciocchi and J. R. Long, *Nature*, 2015, **527**, 357.
- 6 C. R. Martin, G. A. Leith and N. B. Shustova, *Chem. Sci.*, 2021, **12**, 7214–7230.
- 7 S. L. Hanna, S. Chheda, R. Anderson, D. Ray, C. D. Malliakas, J. G. Knapp, K. ichi Otake, P. Li, P. Li, X. Wang, M. C. Wasson, K. Zosel, A. M. Evans, L. Robison, T. Islamoglu, X. Zhang, W. R. Dichtel, J. F. Stoddart, D. A. Gomez-Gualdron, L. Gagliardi and O. K. Farha, *Chem*, 2022, **8**, 225–242.
- 8 A. M. Hastings, D. Ray, W. Jeong, L. Gagliardi, O. K. Farha and A. E. Hixon, *J. Am. Chem. Soc.*, 2020, **142**, 9363–9371.
- 9 S. E. Gilson, P. Li, J. E. S. Szymanowski, J. White, D. Ray, L. Gagliardi, O. K. Farha and P. C. Burns, *J. Am. Chem. Soc.*, 2019, **141**, 11842–11846.
- 10 S. E. Gilson, M. Fairley, S. L. Hanna, J. E. S. Szymanowski, P. Julien, Z. Chen, O. K. Farha, J. A. Laverne and P. C. Burns, *J. Am. Chem. Soc.*, 2021, **143**, 17354–17359.
- 11 Z. J. Li, X. Guo, J. Qiu, H. Lu, J. Q. Wang and J. Lin, *Dalt. Trans.*, 2022, **51**, 7376–7389.
- 12 Z. W. Huang, K. Q. Hu, L. Mei, D. G. Wang, J. Y. Wang, W. S. Wu, Z. F. Chai and W. Q. Shi, *Inorg. Chem.*, 2022, **61**, 3368–3373.
- 13 Z. J. Li, Y. Ju, Z. Zhang, H. Lu, Y. Li, N. Zhang, X. L. Du, X. Guo, Z. H. Zhang, Y. Qian, M. Y. He, J. Q. Wang and J. Lin, *Chem. – A Eur. J.*, 2021, **27**, 17586–17594.
- 14 Z. J. Li, M. Lei, H. Bao, Y. Ju, H. Lu, Y. Li, Z. H. Zhang, X. Guo, Y. Qian, M. Y. He, J. Q. Wang, W. Liu and J. Lin, *Chem. Sci.*, 2021, **12**, 15833–15842.
- 15 J. S. Geng, K. Liu, Y. Y. Liang, J. P. Yu, K. Q. Hu, L. H. Yuan, W. Feng, Z. F. Chai, L. Mei and W. Q. Shi, *Inorg. Chem.*, 2021, **60**, 8519–8529.
- 16 C. F. Baes, N. J. Meyer and C. E. Roberts, *Inorg. Chem.*, 2002, **4**, 518–527.
- 17 C. Ekberg, Y. Albinsson, M. J. Comarmond and P. L. Brown, *J. Solut. Chem.* 2000 291, 2000, **29**, 63–86.
- 18 D. Das and S. R. Bharadwaj, Eds., *Thoria-based Nuclear Fuels*, Springer London,

- London, 2013.
- 19 J. Serp, M. Allibert, O. Beneš, S. Delpech, O. Feynberg, V. Ghetta, D. Heuer, D. Holcomb, V. Ignatiev, J. L. Kloosterman, L. Luzzi, E. Merle-Lucotte, J. Uhlíř, R. Yoshioka and D. Zhimin, *Prog. Nucl. Energy*, 2014, **77**, 308–319.
  - 20 J. Lin, J. N. Cross, J. Diwu, N. A. Meredith and T. E. Albrecht-Schmitt, *Inorg. Chem.*, 2013, **52**, 4277–4281.
  - 21 J. Lin, M. Qie, L. Zhang, X. Wang, Y. Lin, W. Liu, H. Bao and J. Wang, *Inorg. Chem.*, 2017, **56**, 14198–14205.
  - 22 Z. J. Li, S. Guo, H. Lu, Y. Xu, Z. Yue, L. Weng, X. Guo, J. Lin and J. Q. Wang, *Inorg. Chem. Front.*, 2019, **7**, 260–269.
  - 23 P. Li, X. Wang, K. I. Otake, J. Lyu, S. L. Hanna, T. Islamoglu and O. K. Farha, *ACS Appl. Nano Mater.*, 2019, **2**, 2260–2265.
  - 24 J. H. Cavka, S. Jakobsen, U. Olsbye, N. Guillou, C. Lamberti, S. Bordiga and K. P. Lillerud, *J. Am. Chem. Soc.*, 2008, **130**, 13850–13851.
  - 25 C. Falaise, J. S. Charles, C. Volkringer and T. Loiseau, *Inorg. Chem.*, 2015, **54**, 2235–2242.
  - 26 S. Takao, K. Takao, W. Kraus, F. Emmerling, A. C. Scheinost, G. Bernhard and C. Hennig, *Eur. J. Inorg. Chem.*, 2009, **2009**, 4771–4775.
  - 27 C. Hennig, S. Takao, K. Takao, S. Weiss, W. Kraus, F. Emmerling and A. C. Scheinost, *Dalt. Trans.*, 2012, **41**, 12818–12823.
  - 28 K. E. Knope, R. E. Wilson, M. Vasiliu, D. A. Dixon and L. Soderholm, *Inorg. Chem.*, 2011, **50**, 9696–9704.
  - 29 P. Li, S. Goswami, K. I. Otake, X. Wang, Z. Chen, S. L. Hanna and O. K. Farha, *Inorg. Chem.*, 2019, **58**, 3586–3590.
  - 30 Y. B. Wu, C. Xiong, Q. Y. Liu, J. G. Ma, F. Luo and Y. L. Wang, *Inorg. Chem.*, 2021, **60**, 6472–6479.
  - 31 V. V. Butova, A. P. Budnyk, K. M. Charykov, K. S. Vetlitsyna-Novikova, C. Lamberti and A. V. Soldatov, *Chem. Commun.*, 2019, **55**, 901–904.
  - 32 M. C. Wasson, K. Otake, X. Gong, A. R. Strathman, T. Islamoglu, N. C. Gianneschi and O. K. Farha, *CrystEngComm*, 2020, **22**, 8182.
  - 33 T. Islamoglu, D. Ray, P. Li, M. B. Majewski, I. Akpınar, X. Zhang, C. J. Cramer, L. Gagliardi and O. K. Farha, *Inorg. Chem.*, 2018, **57**, 13246–13251.

